Geophys. J. Int. (2010) **181,** 250–260 doi: 10.1111/j.1365-246X.2010.04510.x

A novel weighting method for satellite magnetic data and a new global magnetic field model

Alan W. P. Thomson, Brian Hamilton, Susan Macmillan and Sarah J. Reay

British Geological Survey (NERC), West Mains Road, Edinburgh, EH9 3LA, *UK. E-mail: awpt@bgs.ac.uk*

Accepted 2010 January 7. Received 2010 January 5; in original form 2009 January 23

SUMMARY

A new data weighting scheme is introduced for satellite geomagnetic survey data. Data weights for individual satellite samples at 20-s spacing are derived from two 'noise' (or unmodelled signal) estimators for the sample. First, the standard deviation along the 20 s of satellite track, centred on each sample, is computed as a measure of local magnetic activity. Second a larger-scale noise estimator is defined in terms of a 'local area vector activity' (LAVA) index for the sample. This is derived from activity measured at the geographically nearest magnetic observatories to the sample point. Weighting of the satellite data by the inverse-sum-of-squares of these noise estimators then leads to a robust model of the field, the 'Model of Earth's Magnetic Environment 2008', or MEME08, to about spherical harmonic degree 60. Our approach allows vector samples of the field to be used at all magnetic latitudes and, for example, results in a lithospheric magnetic field model with low spectral noise, comparable with other recent global models. We also do not require a particularly complex model parametrization, regularization, or prior data correction to remove estimates of unmodelled source fields.

Key words: Inverse theory; Satellite magnetics.

1 INTRODUCTION, DATA SELECTION AND MODEL PARAMETRIZATION

Global geomagnetic field research and modelling has been stimulated in the past decade by the Ørsted, CHAMP and SAC-C satellite magnetic survey missions. In particular the quantity and high quality of survey data now available for studying the Earth's magnetic field has allowed greater resolution of internal and external sources of the measured field. In the recent literature, questions of satellite data selection, filtering and treatment have been major areas of study, particularly in attempts to isolate the internal field of the Earth and for revealing details of core processes and of lithospheric structure. Recently, published models range from relatively simple representations of the internal field, for example, the International Geomagnetic Reference Field, version 10 (Macmillan & Maus 2006), to the 'Comprehensive Model' of Sabaka *et al.* (2004), which contains representations of major internal and external field sources, including the quiet, solar-induced magnetic variation of the ionosphere and a representation of field aligned current systems. More developed magnetospheric field models have also been made possible, for example, Maus & Lühr (2005), that model the quiet-time magnetospheric field in an appropriate sun-fixed coordinate system, rather than the geocentric system widely used by the global geomagnetic modelling community.

Thomson & Lesur (2007) (hereafter referred as TL)—the paper on which the work reported here is based—described the global geomagnetic field model BGS/G/L/0706. In deriving BGS/G/L/0706, TL were concerned with improving satellite magnetic data selection techniques, for example by examining the spectral characteristics of models derived according to different data selection criteria. TL experimented to find the best use of magnetic activity indices for Ørsted and CHAMP satellite data, depending on geomagnetic latitude. TL also examined the use of selection filters based on the solar zenith angle and solar wind data and experimented with the vector data and local time (night-side) cut-offs. TL used a two-stage satellite data selection method where the magnetically 'quietest' data, according to the best combination of data filters, were supplemented with a 'second-pass' data set, added with weight equal to that of the 'first-pass' data. This second data set was of marginally less-quiet data. These second-pass data were added to improve both the geographical and temporal distribution (considered year-by-year) of the satellite data used in field modelling.

TL demonstrated that the resultant global model was probably robust up to around spherical harmonic degree 50, based on evidence such as the good coherence observed with other published models, such as CHAOS (Olsen *et al.* 2006) and MF4 (Maus *et al.* 2006). TL noted however that the absence of the southern polar cap index *PCS* after 2003 led to a lithospheric field model for the southern polar cap that was demonstrably corrupted by external field noise.

In this paper we use exactly the same data selection characteristics used by TL and a similar parametrization, for example. a piecewise

linear secular variation and a vector magnetic disturbance (*VMD*) index dependence of external terms. The magnetic index and other data filters for first (second) pass data sets used here and by TL are (definitions and full details in table 1 of TL, 2007):

(i) *Magnetic Indices:* Abs(d*Dst*/dt) $\leq$ 7(20) nT/hour; Abs(d*VMD*/dt) $\leq$ 7(20) nT/hour; Sector-*A* $\leq$ 2-(2+); 0(0) $\leq$ *IE* $\leq$ 30(100) nT; 0(0) $\leq$ *PC* $\leq$ 0.2(1.0) mV/m;

(ii) *Solar Wind Data:* 0(0) $\leq$ *IMF Bz* $\leq +6(+10)$ nT; $-3(-10) \leq$ *IMF By* $\leq +3(+10)$ nT; $-10(-10) \leq$ *IMF Bx* $\leq +10(+10)$ nT; 0(0) $\leq$ *IMF Speed* $\leq$ 450(450) km s^{-1};

(iii) *Other Data:* Solar zenith angle filter for polar cap ($\geq$70 degrees geomagnetic latitude) data only; Otherwise 22:00 $\leq$ Local Time (hr:min) $\leq$ 05:00;

(iv) 2σ (4σ) data residual filter with respect to an earlier BGS model, derived in 2008, where the standard deviation (*SD*) (sigma) was determined from the fit of that earlier model to its data.

However we have both added to and amended the data set used by TL, in the following way:

(i) CHAMP and Ørsted vector and scalar data, where available, were used between 1999 and 2007 inclusive (TL used 2001.0–2005.0);

(ii) CHAMP data were used at calibration level version 50 (downloaded from the CHAMP Science Data Centre in early 2008);

(iii) Quiet, night-time (01:00 to 02:00 LT) hourly means from observatories were used, with the intention of stabilizing secular variation estimates.

Unlike the model of TL, in this paper the second pass data are given a relative weight, as compared with the first pass data (following a suggestion of Nils Olsen). We use a weight factor of 0.2. This best-fitting weight was determined by examining the fit of model to the combined first and second pass data set, as the weight was varied between zero and one. Our trade-off analysis probably produces a best-fitting weight that is a property of these two satellite data sets and of the level of external field noise present. For other data sets and other times the best relative weight may well be different. This weight factor (0.2) is applied to all second-pass data in addition to any other weights described below. We also use 6 nT zenith angle weighting and one-degree tesseral sampling, exactly as in the manner of Lesur *et al.* (2005), who used 5nT zenith angle weight and five-degree tesserae.

In terms of parametrization, TL used a spherical harmonic model where the field **B** was defined in terms of a potential V, such that $\mathbf{B} = -\nabla V(\theta, \phi, r, t)$ and where V contained terms representing:

(i) A degree 15 internal field, with piecewise-linear secular variation assumed and four nodes spaced 1 yr apart at mid-year points (2001.5–2004.5).

(ii) A degree 16–60 static internal field.

(iii) A degree 1 external field, with both *VMD* dependence and a piecewise-linear time variation, with four nodes spaced 1 yr apart at mid-year points, and individual terms representing 24 hr, semi-annual and annual periodicities.

In this paper, we have modified the TL scheme by limiting the linear time dependence of our internal field model to degree 13. We have extended the static (lithospheric) component of our initial models from degree 14 out to degree 100. However we truncate our final model to a maximum degree determined, primarily, by the coherence observed with recent models, in particular xCHAOS (Olsen & Mandea 2008), GRIMM (Lesur *et al.* 2008) and MF6 (Maus *et al.* 2008). As with TL, the emphasis in this paper is on the recovered lithospheric field above about degree 15.

Our model is solved with seven iterations using an L1 norm. The total number of parameters in our model is 5205, compared with 4815 for TL, 315 of which describe external variations and their induced effects. There are seven nodes in our linear secular variation model of internal and external fields, positioned at 2000.0, 2001.5, 2003.0, 2004.5, 2005.5, 2006.5 and 2007.5, with the temporal distribution chosen according to relative numbers of selected satellite and observatory data observed versus time.

In Section 2, we describe the novel weighting scheme used for the satellite data. We note that this weighting is specifically not used for observatory data, as the weights are derived from observatory measurements. In Section 3, we present test model misfits demonstrating the value of vector data at all latitudes and the weighting scheme we have used. In Section 4, we then present the core and lithospheric model MEME08 ('Model of the Earth's Magnetic Environment 2008' with MEME rhyming with 'theme'), developed from the test models of Section 2 and incorporating observatory data. We demonstrate the model's coherence with recently published models and its low lithospheric power spectrum. We conclude that MEME08 is robust to around degree 60 and, in particular, that the weighting scheme helps to overcome small-scale external field corruption of the internal field model, for example at high latitudes.

2 NOVEL SATELLITE DATA WEIGHTING

Additional data weights are defined for each satellite sample separately for each of the vector components of the measured field. This new multiplicative data weight (W) for any given sample is the inverse sum-of-squares of two terms: $W = 1/(SD*SD+\text{LAVA}*\text{LAVA})$. The first term is the sample *SD* in nT. The sample *SD* is an estimate of the sample variability or uncertainty along the track, due to local field sources (although it may also reflect inherent sample noise arising from the magnetometer). The second term in the data weight is the satellite's LAVA index. This is dimensionless by construction and is given on a scale of zero to ten. The LAVA index is intended to quantify larger-scale magnetospheric activity at the satellites ground position, as independently measured by magnetic observatories. (*Note:* In future work, we will investigate whether it is possible to provide the sample *SD* in a normalized and dimensionless form, or compute a LAVA-like index in nT. Here however we consider simply an ad hoc approach to their combination.)

2.1 Sample standard deviation

Fig. 1 illustrates the concept of the sample *SD* as a measure of localized external field activity. As in TL, satellite data are selected for field modelling at a 20-s sampling interval, from the basic 1-s measurement data sets provided by the satellite data centres. The *SD* is then computed from the twenty measurements centred on the sample point, that is, on a track segment of around 150 km length. We do not use the track segment mean as that would introduce a smoothing to the data (but might minimize any risk of sample bias). The mean level may be an appropriate choice for other applications, as might a different sample rate or segment length (although we have not examined this further). However any distinction between individual sample and the segment mean is probably not significant here, as the maximum spherical harmonic degree of our models is of order 70–100 (wavelengths of 571–400 km).

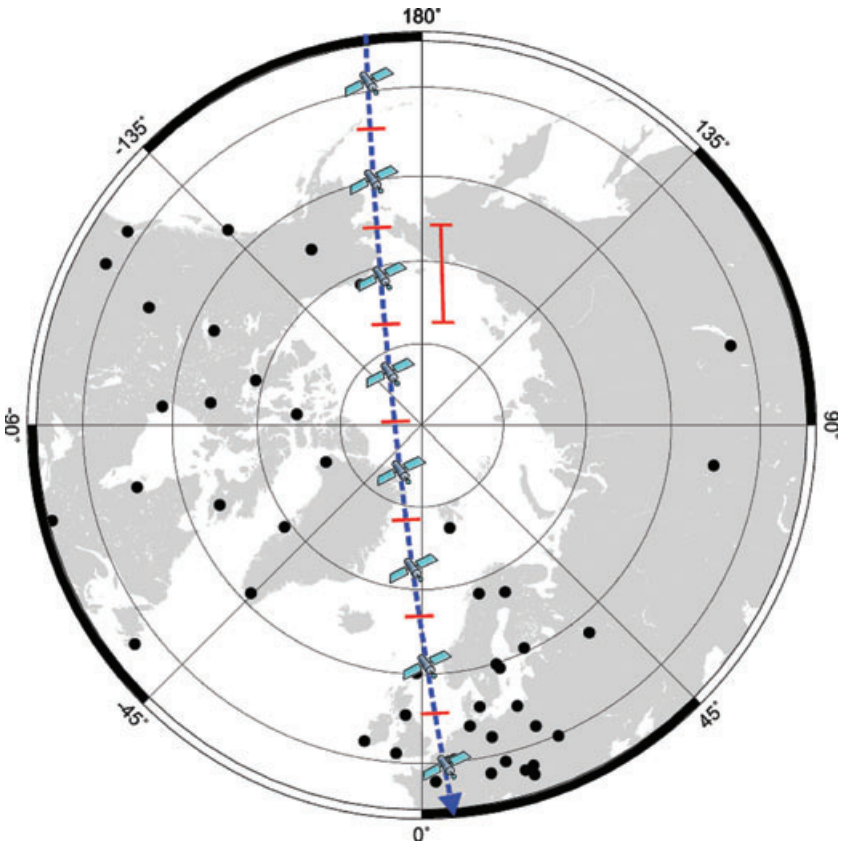

Figure 1. Illustration of the sample standard deviation method, calculated from 20 successive 1-s measurements (e.g. as indicated by the red line segment) along a given polar satellite track (dashed), centred on a particular sample used in field modelling (e.g. as indicated by satellite symbols). INTERMAGNET observatory locations are also shown.

2.2 The LAVA magnetic index

The LAVA index is designed to capture rapid external field variations particularly, but not exclusively, at high latitudes and also where other magnetic index data for satellite data filtering are currently sparse or even absent. LAVA was motivated by the absence of PCS index data after 2003 and the impact this had in the BGS/G/L/0706 model. The INTERMAGNET database contains data from about one hundred magnetic observatories, unevenly distributed across the Earth (see also Fig. 1). The time resolution of INTERMAGNET data is one minute and this is certainly appropriate for rapid variations in the polar ionosphere and in associated field-aligned current systems. INTERMAGNET data are also, of course, independent of any satellite measurement, so can serve as independent estimators of magnetic activity 'near' the satellite ground track.

In constructing the LAVA index for any observatory in the database we first determine the external variation field by subtracting a quiet night-time level from the observatory data. This quiet level is determined using the same principles as used in the derivation of the *AE* index (Mayaud 1980): it is the average for each vector component over the five quietest days of each month. The quiet days are determined from the monthly 'International Quiet Days' identified by ISGI on behalf of IAGA (http://www.cetp.ipsl.fr/isgi/homepag1.htm). (This simple definition of 'quiet level' will introduce a step in quiet levels between successive months. Although expected to be small, month-to-month, the consequences of this step may be examined in future work.) We then determine the *absolute* difference between the quiet level and the measured field at each minute, for each vector component, and for each observatory, over the duration of the model. We bin these absolute variations to construct cumulative probability density curves for each observatory.

Fig. 2 demonstrates the results of this procedure for the Hartland and Lerwick observatories. In general, the probability curves for different observatories differ primarily according to latitude. The probability function slope is typically less steep, as a function of activity level, for observatories at higher latitudes. We determine the deciles of each distribution and these determine the integer values of the LAVA index. In practise, we use 1/2-integer levels to give a finer resolution (further experimentation may be appropriate here). Having defined the LAVA index scale for any observatory we can then read off the nearest index equivalent for any particular absolute value of variation. For example, in Fig. 2, an absolute-value variation of 20 nT in the *X* (north) component would correspond to a LAVA index of about 7.5 for Lerwick and 8.5 for Hartland. Thus a given value of the LAVA index has a different meaning in terms of actual variation in nT, as with observatory *K* indices.

In summary, the LAVA index for any given observatory at any time is determined by

(i) Compute absolute residuals in nT, with respect to an appropriate quiet level, for each vector component and the scalar magnitude separately, over the time span of the data set.

(ii) Construct cumulative probability curves from all residuals, separately for each vector component and the scalar magnitude.

(iii) Determine the deciles of these distributions.

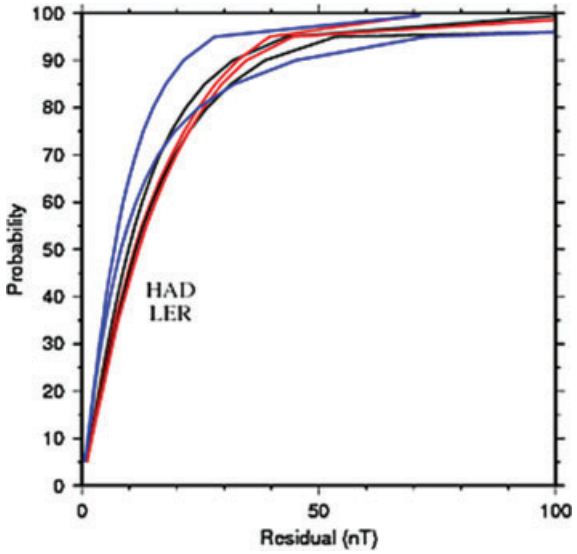

Figure 2. Illustration of LAVA index calculation for each observatory. The absolute value of the variation field, minute-by-minute, is accumulated to form a probability density function in each component at each observatory. Here Lerwick and Hartland data are shown for the *X* (north), *Y* (east) and *Z* (down) field components in blue, red and black, respectively, for data from 2001 to 2004. The higher latitude observatory (Lerwick) has the more gently sloping curves, for a given component/colour.

(iv) Read off the LAVA index from the distribution (e.g. Fig. 2, left hand probability scale divided by ten) for any individual magnetic residual, and for any component, at any given time (e.g. Fig. 2, lower axis).

To define the *satellite* LAVA index, at the given time and position, we then interpolate (weighted by inverse distance) the LAVA indices from the three nearest observatories to the geographic ground position of the satellite, as shown in Fig. 3. From Fig. 3 we see that sometimes these observatories are geographically close to the satellite position. In this case we might expect the interpolated LAVA index to be a useful estimate of the satellite variation field. Sometimes, though, the observatories are widely spaced and the interpolation is probably less useful.

There are some subtle points in the algorithm. First, if data are only available from one or two of the three nearest observatories, we use just these one or two observatories. If none of the nearest three observatories have useable data we give the sample the highest LAVA value, that is, it is heavily down-weighted. However this turns out to be a relatively rare occurrence. The second point is that we interpolate the observatory LAVA indices weighted by their inverse-distance from the satellite ground position. This will therefore preferentially weight the data from the closest observatory, which seems physically reasonable.

Clearly, the LAVA index algorithm is an *ad hoc* approach to independently determining the 'local' (and unmodelled) external field variation observed by satellites. For example, we effectively remove any latitude dependence of variations recorded at observatories by translating to an 'index' via the cumulative probability density. We therefore interpolate like-quantities between observatories, weighted by a simple distance measure for up to three nearest observatories. The algorithm has, however, the advantage of being relatively simple and the results suggest the approach has merit. In particular we find that we can work with vector magnetic data at all latitudes.

Although the method appears worthwhile, since it is *ad hoc* it will have limitations. For example the LAVA index, being derived from ground-based data, may not sense toroidal fields due to field-aligned currents sampled at satellite altitude. On the other hand, active field-aligned currents will presumably disturb the along-track satellite *SD* and may therefore be captured by the sample *SD* in particular vector components.

3 MODEL COMPARISONS

In Table 1, we show the weighted Gaussian misfit of five models fit to a data set derived from satellite data only. (Satellite-only data were used here simply for convenience: the final MEME08

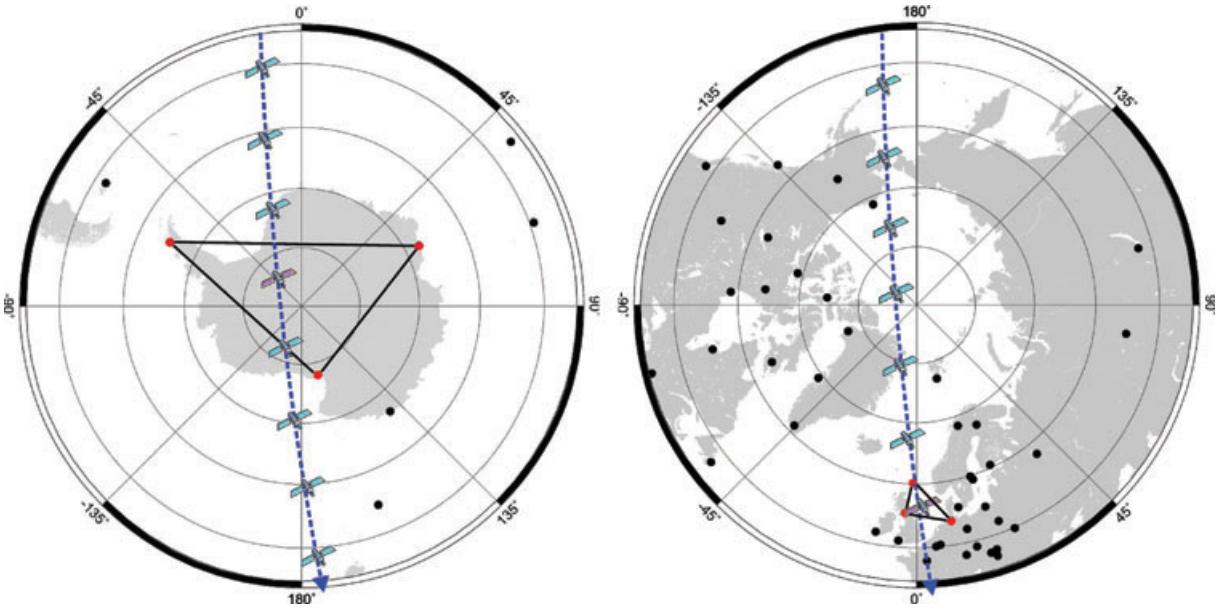

Figure 3. The satellite LAVA index is interpolated and relatively weighted by inverse-distance from the observatory LAVA indices at up to three geographically nearest-neighbour INTERMAGNET observatories. These examples for southern (left-hand panel) and northern (right-hand panel) high latitudes demonstrate the typical spatial distribution of observatories and hence give a sense of the likely varying accuracy of the LAVA index method over different regions of the Earth.

Table 1. Standard deviation misfit for five models fit to the combined first- and second-pass *satellite-only* data sets.

Model number	Weighted misfit	X'	Y'	Z'	F	Model description
1	1.00	3.50	3.50	3.97	3.88	Baseline: Includes second pass data weight (0.2); No further weighting
2	0.94	3.53	3.58	3.97	3.75	As 1, also weighted by *SD*; Scalar data only above 50 deg.
3	0.91	3.59	3.61	4.01	3.68	As 1, also weighted by *SD*; Vector data at all latitudes.
4	0.64	3.49	3.53	3.92	3.41	As 1, also weighted by *SD* and LAVA; Scalar data only above 50 deg.
5	0.62	3.56	3.59	4.00	3.51	As 1, also weighted by *SD* and LAVA; Vector data at all latitudes.

Notes: These models differ according to whether data weighting is applied to the satellite sample and whether vector or only scalar data are used above 50 degrees geomagnetic latitude, as given in the 'Model description'. The weighted L2 misfit (dimensionless) is given in the second column. X', Y', Z', F unweighted misfits (nT) to satellite data in geocentric-solar-magnetospheric coordinates are also given (where the X'-axis points towards the Sun and the Z'-axis is the projection of the Earth's magnetic dipole axis (positive north) on to the plane perpendicular to the X'-axis).

model—Section 4—contains both satellite and observatory data.) Model 1 is our 'baseline': the first- and second-pass data samples are used with no weighting by *SD* or by LAVA. However, we do apply a relative weight of 0.2 for the second pass data, as described before. The weighted L2 misfit of model 1 is 1.0 (a consequence of the choice of relative weight, 0.2, between the data sets). Models 2–5 then show the impact of applying just the inverse square *SD* weight to the data sample (for models 2 and 3), or the inverse sum of squares of *SD* and LAVA for the sample (for models 4 and 5). Models 2 and 3 (and models 4 and 5) then differ only in terms of whether scalar data are used above 50 degrees geomagnetic latitude, or whether full vector data are used at all latitudes.

The lowest overall weighted misfit (0.62) is found with model 5. This suggests that this combination of *SD* and LAVA weighting

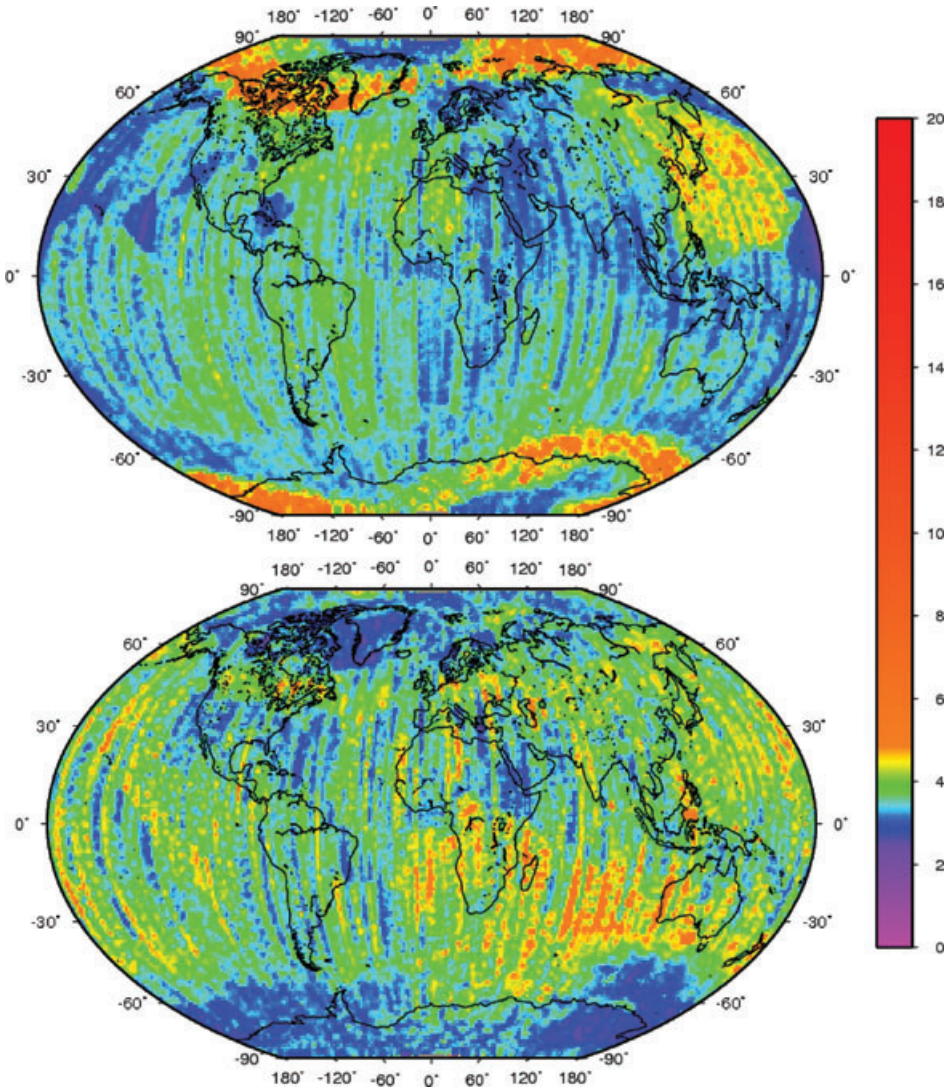

Figure 4. The geographical distribution of the combined standard deviation and LAVA down-weight factors $W^{-1/2}$ for X (top panel) and Z (bottom panel) component CHAMP data, averaged in one degree bins over all years of the model.

is the most useful and that neither individual weight is particularly dominant. However the model weights change from model 1 to model 5 so the comparison, in terms of weighted misfit, is only one measure of model suitability. We also find that introducing vector data at high latitudes does not necessarily produce problems in the misfit, as the vector misfit *SD* (columns 3–5 Table 1) does not markedly change between models 1 and 5.

In understanding the impact of the *SD* plus LAVA weighting scheme on models, it is instructive to examine the geographical distribution of the combined weights that have been applied to the measurements. In Fig. 4 we show the inverse square root of the weight ($W^{-1/2}$, with W defined as before) that defines the down-weighting applied to the X (north) and Z (vertical) components of the field sampled by the CHAMP satellite, for 2001–2007. The distribution of the down-weight factor for Y (east) is generally similar to that of X, but it lacks the prominent down-weight over the northwest Pacific region. The auroral zones are clearly picked out by the method, as one might have expected, but there is, for example, no equatorial electrojet signature (however we use night-side data only and there are few observatories close enough to this electrojet to sample its effect). At mid and low latitudes the weighting scheme can be seen to pick out particular satellite tracks and groups of measurements as being, according to the method, 'noisy'. However other than the auroral signal in Fig. 4 it is not obvious that the other 'noisy' patches have any physical significance, e.g. in terms of known current systems. Indeed heavier down-weighting could be a consequence of large gradients in the core and lithospheric field over each 20-s track segment and, of course, any problems with data from particular observatories. Further work is therefore suggested here.

4 MEME08

Based on the test models described above, the 2008 'Model of the Earth's Magnetic Environment' (MEME08) is constructed from vector satellite data at all latitudes and with the satellite data weighting of Section 2 applied. Observatory hourly means are also used and are given a weight proportional to the mean satellite weight, to avoid any possible heavy up- or down-weighting relative to the satellite data. MEME08 spans 1999–2007 and contains a piecewise-linear secular variation model for internal and external terms. The initial 'parent' model is derived to degree 100 but is truncated to degree 60 for reasons described below.

The power spectrum of the core field and secular variation of the MEME08 model, to degree 13 is shown in Fig. 5, in comparison with xCHAOS (Olsen & Mandea 2008) and GRIMM (Lesur *et al.* 2008), all at epoch 2004.0. The power spectrum of the lithospheric field (degree 14–70) is then shown in Fig. 6, in comparison with BGS/G/L/0706 (Thomson & Lesur 2007), xCHAOS, GRIMM and MF6 (Maus *et al.* 2008). In Figs 7–10, we show, respectively, the degree coherence observed between models, various percentage normalized coefficient sensitivity matrices, and geographical maps of the lithospheric vertical down (Z) field and field differences at the Earth's surface (see Olsen *et al.* 2006) and Langel & Hinze (1998) for coherency and sensitivity function definitions). In Figs 6–9 all models are evaluated at epoch 2002.0 to account for any difference in the maximum secular variation degree in each case. The fit of the MEME08 model to satellite and observatory data is given in Table 2.

From Fig. 6 it is clear that truncating the model to around degree 60 is probably appropriate. The power spectrum starts to show a

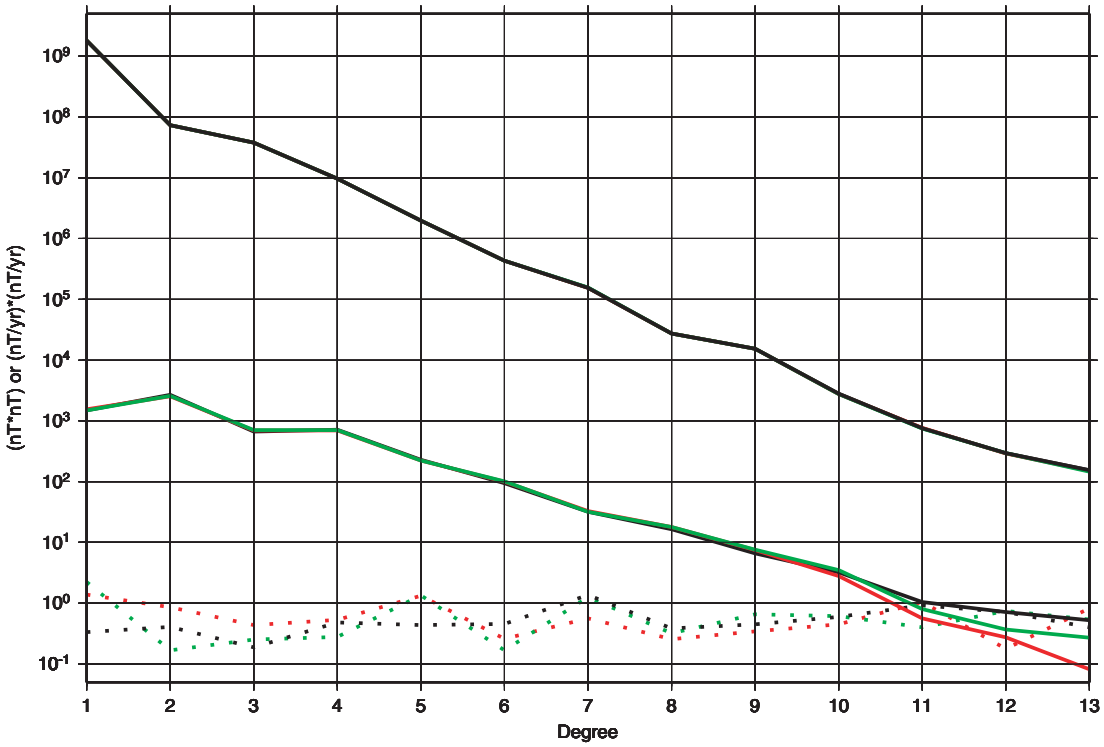

Figure 5. Power spectrum (degree 1–13) of the MEME08 model (upper black curve), xCHAOS (red) and GRIMM (green). Core field power spectrum differences of MEME08 with respect to xCHAOS (red dashed) and GRIMM (green dashed) and between xCHAOS and GRIMM (black dashed) are given. Also shown are the secular variation spectra of the three models (lower solid lines: MEME08-black, xCHAOS-red and GRIMM-green). Figures drawn for epoch 2004.0.

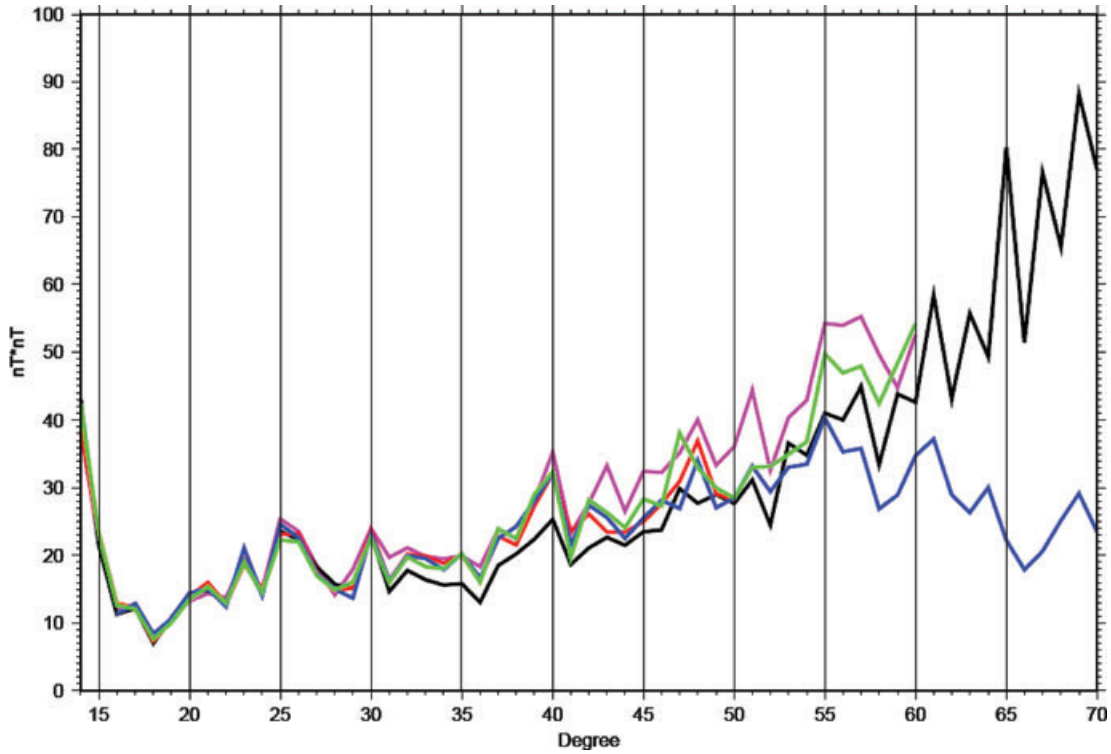

Figure 6. Power spectra (degree 14–70) of the MEME08 model (black) and of the BGS/G/L/0706 (purple), xCHAOS (red), GRIMM (green) and MF6 models (blue), at the Earth's surface.

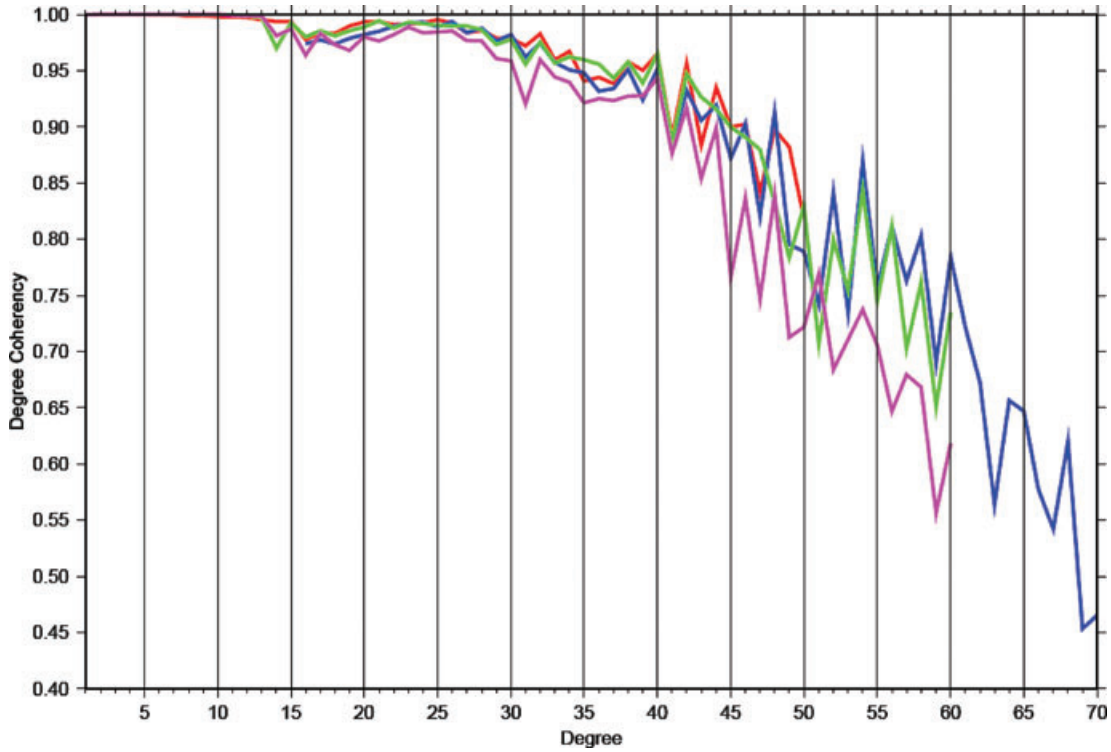

Figure 7. Coherency functions (to degree 70) of the MEME08 model with BGS/G/L/0706 (purple), xCHAOS (red), GRIMM (green) and MF6 (blue).

clear upwards bend in the region of degree 60–70, as model coefficients presumably become less constrained by data. The coherency and sensitivity data would also suggest that MEME08 is robust to around degree 60 and that it improves on BGS/G/L/0706.

We note the following other characteristics in the power spectra, coherency, sensitivity matrix and lithospheric map data.

(i) *Power spectra:* the core field power spectra of MEME08, xCHAOS and GRIMM are similar (Fig. 5). The power spectra of

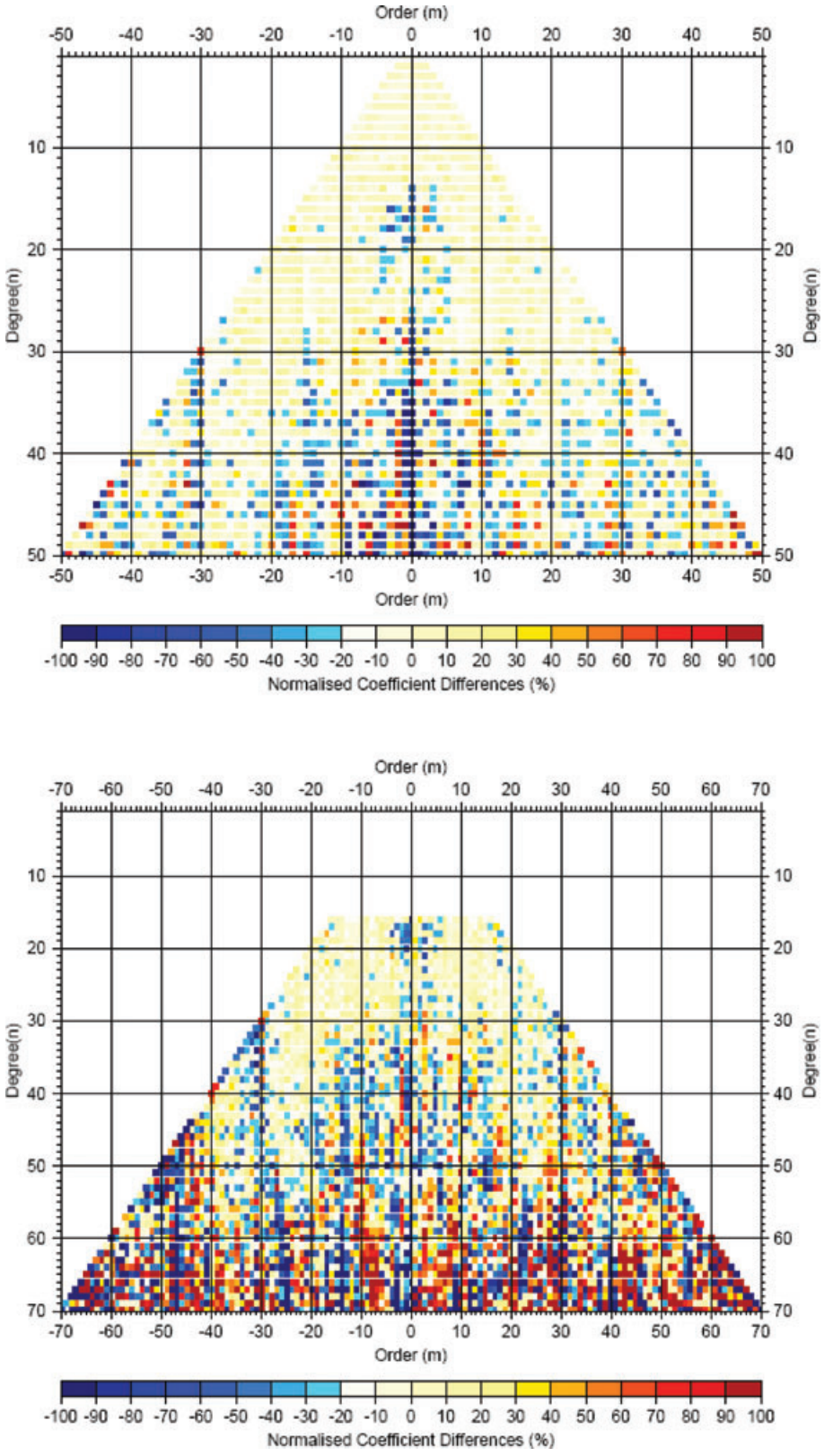

Figure 8. Percentage normalized sensitivity matrices of the MEME08 model, compared with xCHAOS (top panel) and MF6 (bottom panel). Positive/negative order denotes cosine/sine dependence on longitude in the spherical harmonic expansion.

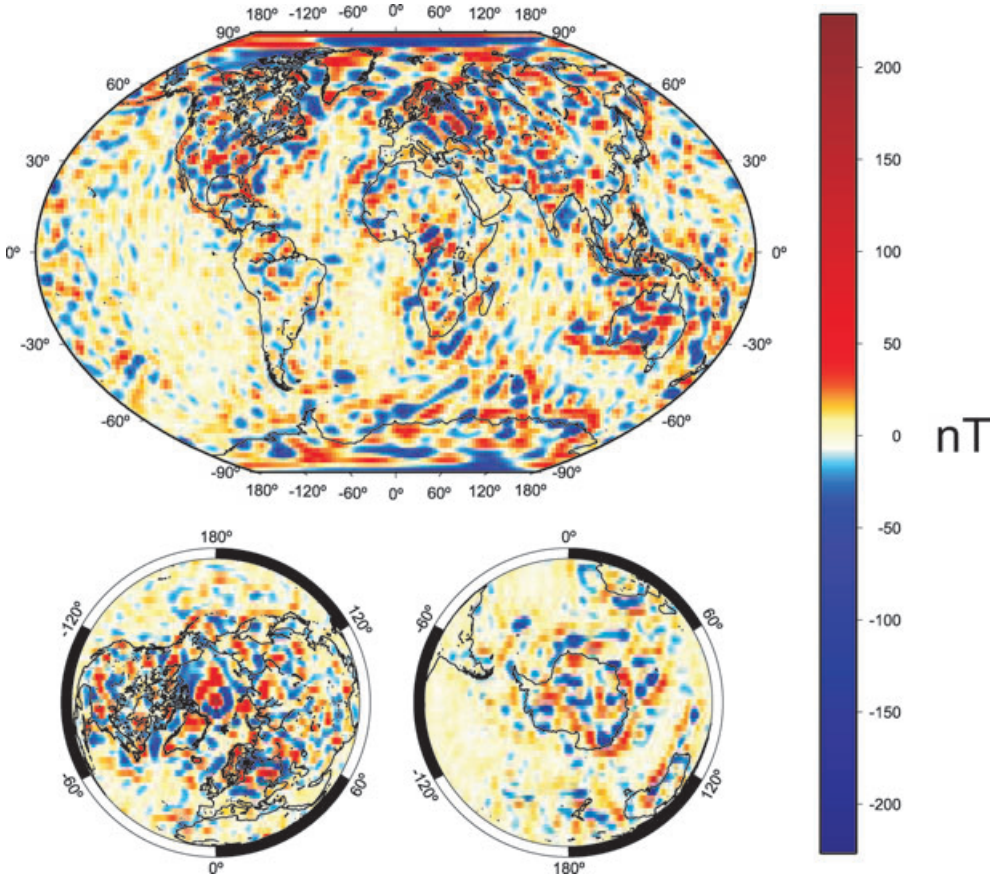

Figure 9. Vertically down lithospheric field at the Earth's surface from the MEME08 model (degree 15–60, in nT).

differences between MEME08 and the other models tend to peak at degrees 1, 5, 7 and 11. Secular variation model differences also become clearer above degree 10. The MEME08 model has a lithospheric power spectrum (Fig. 6) that is systematically lower than other models up to around degree 50–55. However this may be at least partly due to the 2σ data filter applied to satellite data. There are otherwise only small differences in the harmonic structure observed between models and the larger 'oscillations' do not appear until above degree 60. MEME08 has less power at many degrees compared with MF6, which uses along-track filtering. This might then suggest that signal is being removed by our weighting scheme; but it is not obvious how this can happen given that the scale lengths, for example, for the *SD* calculation (about 150 km), is much less than the wavelength of the maximum degree of the model.

(ii) *Coherency:* model coherency (Fig. 7) is generally higher than about 0.90, with respect to all models shown, up to degree 40. To degree 60 (where we think the model is probably robust) the MEME08 model has a coherency above 0.60 with respect to other models. By about degree 70 the coherency with MF6, the only other model to this degree, drops to about 0.5.

(iii) *Sensitivity:* Fig. 8 shows the models with which MEME08 agrees most (xCHAOS) and least (MF6). We can see that there is indication of systematic differences in near-zonal and some sectoral terms. However differences are particularly clear in vertical stripes around odd multiples of ten in harmonic order. Otherwise there is the expected general degradation in agreement with increasing harmonic degree. Interestingly, we also see a 'patch' of larger differences for degrees 16–20 and low harmonic order.

(iv) *Lithospheric field:* Fig. 10 shows that at mid latitudes differences between models are largely in the high spherical harmonic orders and to some extent in bands around 30 degrees latitude. In particular we find weaker meridional 'striping' in MEME08 (Fig. 9), compared with GRIMM (*cf* . also the lower relative power in Fig. 6). There is also less power in general in the high latitude magnetic anomalies in the MEME08 model (Fig. 9). However there is a clear maximum in the MEME08 model (Fig. 9) at the northern—but notably not the southern—geographic pole. This appears artificial, at least in comparison with other published models. It is not obviously an artefact of the colour scheme or of the plot resolution used. This feature may reflect the absence of data within a few degrees of the poles, the weak down-weighting by activity level (*cf.* Fig. 4), as well as the lower signal-to-noise ratio from the oceanic anomaly field of the northern polar cap, compared with the field over continental Antarctica. The feature may also be a consequence of the data selection algorithm. Polar characteristics of the model will be examined further in preparing the next generation of MEME.

(v) *Model fit to data:* Table 2 indicates a misfit comparable with other recent models, even though vector data have been used at all latitudes. The satellite data are the dominant contributor to the model but, apart from the *F*-misfit, the fit to observatory data is not significantly poorer than the fit to satellite data. Misfits were computed for degrees 1–60. *Note:* in comparison with Table 1, here we use both satellite and observatory data, hence the larger satellite misfits.

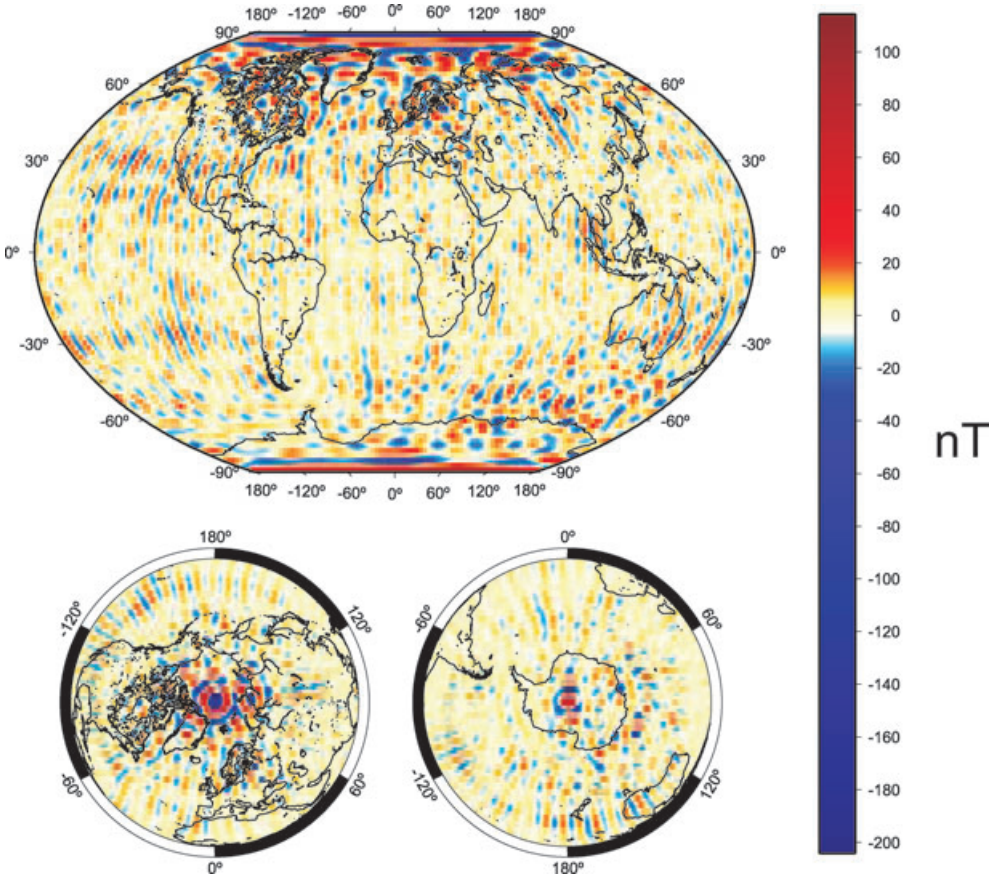

Figure 10. Vertically down lithospheric field difference at the Earth's surface between GRIMM and MEME08 (degree 15–60, in nT).

Table 2. Mean (*SD*) misfit in nT for MEME08 with respect to satellite and observatory data. *X*, *Y*, *Z*, *F* denote the north, east, vertical and total field misfit.

Data type	Data number	*X*	*Y*	*Z*	*F*
Satellite	1915,605	−0.09 (6.64)	0.00 (5.28)	0.09 (4.59)	0.27 (3.98)
Observatory	176,234	−0.03 (8.34)	0.09 (4.49)	−0.04 (5.56)	−0.34 (14.31)

5 SUMMARY AND CONCLUSIONS

MEME08 takes advantage of a novel data weighting approach for satellite field measurements. This approach is based on an independent estimation of the smaller-scale external field variations, considered as a noise source that mixes with the internal field that we primarily wish to recover. That this approach is successful is demonstrated by our ability to use vector samples of the field at auroral and polar latitudes, rather than just the scalar field, as is often the case in global field modelling. The MEME08 lithospheric model is consistent with other recent models that have different approaches to external field rejection and is arguably robust to around spherical harmonic degree 60. MEME08 has a low power spectrum to about degree 55 and has less evidence of along-track 'striping' compared to other models. However, more work is perhaps needed to constrain the model within a few degrees of the geographic poles where satellite and surface data are either unavailable, or where existing satellite data may be relatively down-weighted by the magnetic activity level.

The data weighting scheme was devised with two aims. The first, represented by the *SD*, was an attempt to capture any localized activity from sources not in the model and not rejected by data selection filters based on existing magnetic indices. The LAVA index was then an attempt to measure those larger-scale variations, on spatial scales often well below those spanned by standard magnetic indices and at a time resolution more applicable to the dynamics of the ionosphere, particularly so towards the poles. We have found by experimentation that both data weights are useful although the LAVA index has perhaps more impact on model fit. There may be scope for further investigation of the relative importance of each term but clearly on a pragmatic level the method works. However, given that the method is undoubtedly *ad hoc*, though with some physical motivation, there is clearly scope to devise and experiment with other weighting schemes. We also remark that the external field noise estimates have been used as weights rather than as data selection options. This was done mainly to avoid further decimating satellite data sets used for global modelling, particularly at high latitudes. Further work using these activity measures for data selection may however be worthwhile.

LAVA indices should be readily derivable for non-INTERMAGNET observatories, for example those held in World Data Centre databases, as well as being derivable for variometer stations, given the algorithm and its simple baseline definition. Such data, when

added to INTERMAGNET data, should then definitely improve our ability to determine the localized activity present in satellite data, not least at high latitudes. The global community of ground-based magnetometer networks can therefore be seen to have a major role to play during future satellite magnetic survey missions, such as the planned ESA 'Swarm' mission.

ACKNOWLEDGMENTS

We would like to acknowledge the Ørsted and CHAMP science data centres, INTERMAGNET (at http://www.intermagnet.org) and the institutes running individual INTERMAGNET observatories. We would also like to thank colleagues within the UK 'GEOSPACE' consortium for their comments on this work and thank the referees for comments and suggestions that have improved the paper. This paper is published with the permission of the Executive Director, BGS (NERC) and the work was supported by NERC grant NER/O/S/2003/00677.

REFERENCES

Langel, R.A. & Hinze, W.J., 1998. *The Magnetic Field of the Earth's Lithosphere: The Satellite Perspective,* Cambridge University Press, Cambridge.

Lesur, V., Macmillan, S. & Thomson, A., 2005. Deriving main field and secular variation models from synthetic Swarm satellite and observatory data, *Earth, Planets, Space,* **58,** 409–416.

Lesur, V., Wardinski, I., Rother, M. & Mandea, M., 2008. GRIMM: the GFZ Reference Internal Magnetic Model based on vector satellite and observatory data, *Geophys. J. Int.,* **173,** 382–394, doi:10.1111/j.1365-246X.2008.03724.x.

Macmillan, S. & Maus, S., 2006. International Geomagnetic Reference Field—the tenth generation, *Earth, Planets, Space,* **57,** 1135–1140.

Maus, S. & Lühr, H., 2005. Signature of the quite-time magnetospheric magnetic field and its electromagnetic induction in the rotating earth, *Geophys. J. Int.,* **162,** 319–330, 3, 755–763.

Maus, S., Rother, M., Hemant, K., Stolle, C., Lühr, H., Kuvshinov, A. & Olsen, N., 2006. Earth's lithospheric magnetic field determined to spherical harmonic degree 90 from CHAMP satellite measurements, *Geophys. J. Int.,* **164,** 319–330, doi:10.111/j.1365-246X.2005.02833.x.

Maus, S. *et al.*, 2008. Resolution of direction of oceanic magnetic lineations by the sixth-generation lithospheric magnetic field model from CHAMP satellite magnetic measurements, *Geochem. Geophys. Geosyst.,* **9**(7), doi:10.1029/2008GC001949.

Mayaud, P.N., 1980. *Derivation, meaning and use of geomagnetic indices,* Geophysical Monograph no. 22, American Geophysical Union, Washington.

Olsen, N. & Mandea, M., 2008. Rapidly changing flows in the Earth's core, *Nat. Geosci.,* **1,** doi:10.1038/ngeo203.

Olsen, N., Lühr, H., Sabaka, T.J., Mandea, M., Rother, M., Toffner-Clausen, L. & Choi, S., 2006. CHAOS—a model of the Earths magnetic field derived from CHAMP, Ørsted, and SAC-C magnetic satellite data, *Geophys. J. Int.,* **166,** 6775, doi:10.1111/j.1365-246X.2006.02959.x.

Sabaka, T.J., Olsen, N. & Purucker, M.E., 2004. Extending comprehensive models of the Earth's magnetic field with Ørsted and Champ data, *Geophys. J. Int.,* **159,** 521–547.

Thomson, A.W.P. & Lesur, V., 2007. An improved geomagnetic data selection algorithm for global geomagnetic field modelling, *Geophys. J. Int.,* **169,** 951–963, doi:10.1111/j.1365-246X.2007.03354.x.